Modeling of Damage Initiation and Progression in a SiC/SiC Woven Ceramic Matrix Composite

Subodh K. Mital[1]
The University of Toledo, Toledo, Ohio, 43606, U.S.A.

Robert K. Goldberg[2] and Peter J. Bonacuse[3]
NASA Glenn Research Center, Cleveland, Ohio, 44135, U.S.A.

The goal of an ongoing project at NASA Glenn is to investigate the effects of the complex microstructure of a woven ceramic matrix composite and its variability on the effective properties and the durability of the material. Detailed analysis of these complex microstructures may provide clues for the material scientists who 'design the material' or to structural analysts and designers who 'design with the material' regarding damage initiation and damage propagation. A model material system, specifically a five-harness satin weave architecture CVI SiC/SiC composite composed of Sylramic-iBN fibers and a SiC matrix, has been analyzed. Specimens of the material were serially sectioned and polished to capture the detailed images of fiber tows, matrix and porosity. Open source analysis tools were used to isolate various constituents and finite elements models were then generated from simplified models of those images. Detailed finite element analyses were performed that examine how the variability in the local microstructure affected the macroscopic behavior as well as the local damage initiation and progression. Results indicate that the locations where damage initiated and propagated is linked to specific microstructural features.

I. Introduction

High temperature ceramic matrix composites (CMC) are being explored as viable alternative for hot section gas turbine, airframes and other air breathing propulsion components that are subjected to very high temperatures. However, these materials are heterogeneous and various factors affect their properties in a specific design environment. The microstructure of a woven ceramic matrix composite displays a significant amount of variability and irregularity in aspects such as tow spacing, ply alignment, nesting of adjacent plies and matrix thickness. Furthermore, particularly for chemical vapor infiltrated (CVI) composites, there is a significant amount of porosity arranged in irregular patterns. Therefore, a need exists to investigate the effects of this complex material microstructure on the effective properties and durability of these materials. A need also exists to determine how the characterized variability in the microstructural parameters such as tow shape and size, ply alignment, amount and distribution of porosity correlates with the known variability in CMC material properties.

Generating high-fidelity models of the material microstructure is a challenging task. As discussed in Nemeth, et al.[1] and Mital, et al.[2], in many of the analytical approaches derived to model the response of woven ceramic matrix composites, the representative composite unit cell (the smallest repeating unit that is assumed to be representative of the composite as a whole) has been modeled using a "pristine", ordered architecture with average dimensions for the tow geometry and spacing. In addition, the areas between the fiber tows are assumed to be composed entirely of matrix material. The effects of porosity are accounted for by uniformly degrading the properties of the matrix based on the measured pore volume fraction in the composite. Utilizing these traditional approaches, incorrect predictions of composite properties often occur. For example, as found by Goldberg, et al.[3], the through-thickness modulus has been found to be a function not only of the amount of porosity, but the shape and distribution of the porosity as well. Furthermore, Goldberg, et al.[3] found that models of woven ceramic matrix composites that included more realistic representations of the microstructure provided an improved capability to identify the sites for stress risers where damage is likely to initiate. Traditional techniques, where the porosity is merely smeared with the matrix or

---

[1] Senior Research Associate, Department of Mechanical, Industrial and Manufacturing Engineering
[2] Research Aerospace Engineer, Structures and Materials Division, AIAA Associate Fellow
[3] Materials Research Engineer, Structures and Materials Division

the fiber tows are regularly spaced, can only capture the stress distribution in an average sense as shown by Mital, et al.[2].

The goal of an ongoing project at NASA Glenn is to investigate the effects of the complex microstructure of a woven ceramic matrix composite and its variability on the effective properties and the durability of the material. Detailed analysis of these complex microstructures may provide clues for the material scientists who 'design the material' or to structural analysts and designers who 'design with the material' regarding damage initiation and damage propagation. A model material system, specifically a five-harness satin weave architecture CVI SiC/SiC composite composed of Sylramic-iBN fibers and a SiC matrix, has been analyzed. The objective is to investigate the effects of the complex microstructure on the effective mechanical properties and durability of the composites, including damage initiation and progression, as well as to relate the microstructural variability to the variability in effective properties. A separate effort by the authors involves the development of methods to characterize the distributions in as-fabricated composites of various microstructural parameters such as tow width and spacing, ply nesting, ply misalignment etc. Emphasis was given in the current study to determining the effects of the microstructure on the initiation and growth of damage up to the point of the proportional limit stress. In the design of components using ceramic matrix composites, the proportional limit stress, defined as the stress level where the tensile stress-strain curve deviates significantly from linearity (proportional limit), is often a key material allowable. The variability in constituent material properties, while likely to also be a contributor to the variability in the composite properties, is currently not part of this investigation. The objective of this work is to perform progressive damage analyses on various two-dimensional cross section models to determine the likely sites for damage initiation and to relate the damage patterns to the architectural features of the given section. Determining the correlation between the local damage patterns and the overall stress-strain response of the material was another objective of this work.

II.   Microstructural Characterization

In order to systematically characterize the constituents of the composite and to quantify the variability in composite architectural parameters such as tow shape, size, spacing, porosity size and shapes, relative alignment of plies etc., microstructural characterization of the cross-sections of composite was undertaken. This process involves several steps including quantitative image analyses and collecting high-resolution images of the composite cross-sections. The steps involved in the process are briefly described here. The reader is referred to Ref. 3 for a detailed description of the described parts of the procedure.

A. Serial Sectioning

Samples of the composite were serially polished using a destructive technique and high resolution images were acquired at each polishing step. The target removal rate was 0.2 mm per polishing step. The specimens were initially 12.7 mm square with a thickness of approximately 2 mm. Images of the polished section were acquired with an optical microscope that allowed for automated acquisition of high resolution images of the whole cross-section.

B. Image Segmentation

An automated and repeatable process was developed to gather the statistics needed for generation of analysis models that can quantify the effects of microstructural variability. This process is usually referred to as segmentation. Statistical techniques were used to isolate various constituents in the cross-sections i.e. longitudinal tows, transverse tows, inter-tow matrix and porosity based on the pixel intensities of various constituents in the images acquired in previous steps. With the goal that the capability be readily shared with other researchers, it was decided that this implementation should be open-source. The Python Programming language [http://www.python.org/] was chosen with the addition of image processing and manipulation tools in the SciPy and NumPy libraries [http://www.scipy.org/].

C. Quantitative Image Analysis

This step involves using the information in the segmented images to isolate the microstructural features of interest: transverse section tows, longitudinally sectioned tows, pores and the SiC matrix surrounding the tows. Using certain morphological operations, it was possible to isolate these constituents with reasonable accuracy. In general, these operations took advantage of the fact that the shapes of different microstructural features are different. For example, the fiber coating cluster was chosen for the tow identification because this isolated cluster represented the shapes of the tows best. Figure 1 shows the results of the automated constituent isolation for a section.
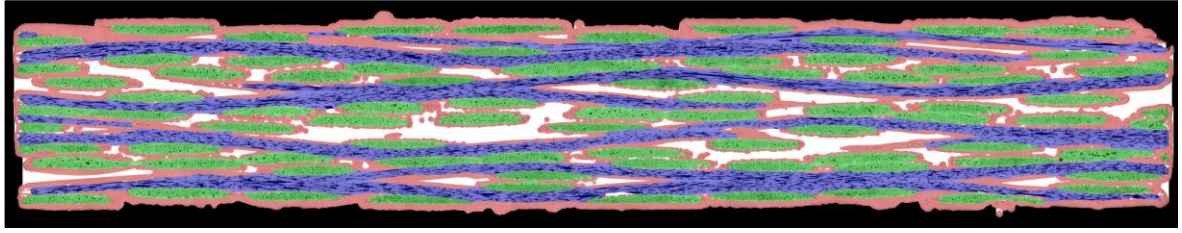
Figure 1. Composite constituents isolated with an automated procedure utilizing binary morphological operations. Isolated constituent overlaid on the image of the cross section. Transverse sectioned tows – green; longitudinally sectioned tows – blue; matrix – red; inter-tow porosity – white; and outside specimen – black.

D. Segmented to Simplified

Usually the images obtained in the previous step by isolating composite microstructures are not amenable to generation of finite element models for analysis due to the very irregular size and shapes of the constituents, ply misalignment etc. Techniques were developed to generate simplified images of the cross-sections while still maintaining the maximum possible relevant microstructural details. Several approximations had to be made. Transverse tows were assumed to be of lenticular shape with an area that is the average of all the transverse tows in the cross-section. The longitudinal tow's path was assumed to be sinusoidal and they were assumed to be of constant thickness, which was calculated as the average value of the thickness of the segmented longitudinal tows in the cross-section. Some of the locations of the transverse tows had to be adjusted in order to minimize interference with the longitudinal tows or other transverse tows. This was also due to the fact that plies have a slight misalignment relative to each other. In addition, the matrix was "grown" uniformly from the tows until the matrix volume fraction matched the volume fraction determined from the segmented image. In real sections, because of the nature of the infiltration process used for these composites, the matrix thickness is higher on the outer edges and is
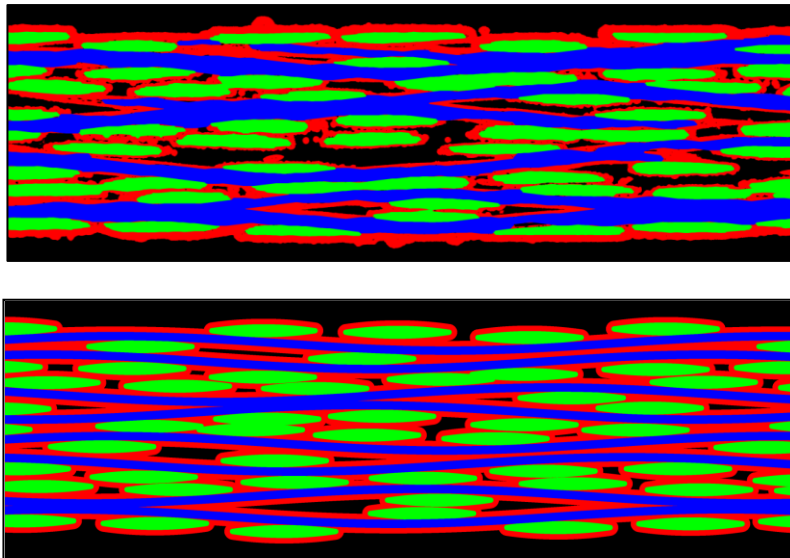

Figure 2. Comparison between a segmented image (top) and a simplified image (bottom) constructed for FEM model generation.

relatively low in the interior of the cross-section. Figure 2 shows a comparison between a segmented image and a simplified image. The process used to generate simplified images led to slight differences in the volume fractions of various constituents between the segmented and simplified images, but the overall nature of the distribution is captured. Most importantly, simplified images can be used to generate finite element models for structural analysis as explained in the following sections.

American Institute of Aeronautics and Astronautics

III. Finite Element Analysis

The simplified two-dimensional sections generated using the serial sectioning methods discussed in the previous sections were analyzed to explore the effects of the complex microstructure. Two-dimensional finite element models of both the actual and artificially generated "aligned" sections were developed using a software tool OOF2 (Objected-Oriented Finite Element Analysis of Material Microstructures)[4]. The "aligned" sections were generated using the fit sinusoidal longitudinal tow shape and regularly spaced transverse tows from the simplified specimens, appropriately arranged for a five-harness satin weave configuration. Those finite element models were then analyzed using the ABAQUS[5] general purpose finite element program. Initially, analyses were performed where the material constituents were assumed to be purely elastic under an in-plane tensile load. The purpose of those analyses was to identify the locations of stress hot-spots as these would most likely be the locations where damage would initiate. Following those analyses, material constituents were modeled as non-linear: initially as elastic-perfectly plastic to allow for stress redistribution following the failure ('yield') of the material and then as brittle which allows for complete stress redistribution and damage progression following the failure. These tools, analyses performed and the results obtained are described in the following sections.

E. Mesh Generation and Model Details

The OOF2 software was used to create the two-dimensional finite element meshes for several of the two-dimensional sections (slices) in this study. Two-dimensional finite element meshes for a few idealized or "aligned"
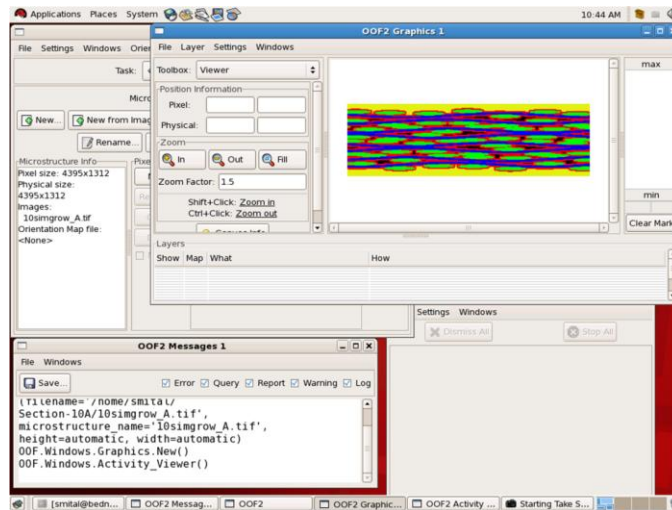

Figure 3. Screenshot of OOF2 graphical user interface

(computer generated) sections were also created for comparison with the actual slices. OOF2 is a public domain software product developed at the National Institutes of Standards and Technology (NIST). OOF2 can generate an appropriate finite element model starting from a two-dimensional representation, or image, of arbitrary geometrical complexity. It can export the finite element meshes generated from the image analysis directly into the ABAQUS finite element program, which can then analyze the model. A screenshot of the OOF2 graphical user interface is
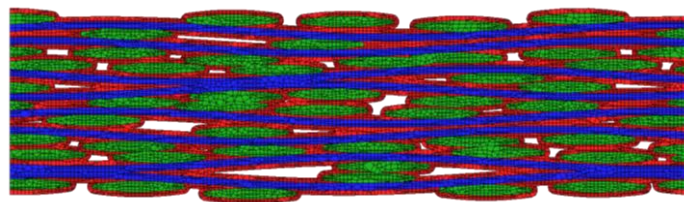

Figure 4. Finite element mesh of a representative cross-section with 17442 nodes and 19502 elements (14545 linear quadrilateral and 4957 linear triangular elements.

shown in Fig. 3. Finite element meshes were generated for many actual and idealized sections. A typical finite element mesh for a representative cross-section is shown in Fig. 4. As before, the displayed section consists of

4

American Institute of Aeronautics and Astronautics

longitudinal (shown in blue) and transverse (shown in green) tows, CVI-matrix (shown in red) and porosity (shown as empty spaces). The longitudinal and transverse tows were treated as homogenized materials in this model even though the tows consisted of fiber, interfacial coating, matrix and intra-tow porosity. The tow properties were calculated using standard micromechanics equations for a unidirectional composite. Room-temperature constituent properties are shown in Table I. Since this intra-tow porosity has been found to be relatively uniformly distributed[3], this porosity was not explicitly modeled but was used in determining the homogenized properties of the tow

Table I. Constituent room-temperature material properties

Tow Properties 800 filament Sylramic-iBN, Filament diameter = 9.5 μm, BN coating thickness = 0.6 μm, 15% porosity (assumed uniformly distributed)	E_{11} = 37.7 Msi (260 GPa) E_{22} = 15.3 Msi (105.5 GPa) ν_{12} = 0.18 G_{12} = 6.2 Msi (42.5 GPa)
CVI-SiC Matrix	E = 61 Msi (420 GPa) ν = 0.2

material.

F. Analysis Results and Discussion

In a previous report[3], the effective in-plane and through-thickness modulus of various cross-sections as well as stress distributions in these sections due to an applied in-plane tensile load were computed [3] using the ABAQUS finite element analysis code. The idea of these analyses, performed in the linear elastic regime, was to identify the patterns of stress distribution, identify the areas of stress risers and to determine if any correlation could be found between the stress distribution and the composite microstructure. The reader is referred to Ref. 3 for the details of those analyses.

Following the linear elastic analyses, efforts to model the progressive damage in several sections were undertaken. The primary focus of that was to determine, for various actual and "aligned" sections, where damage initiated and to relate the damage locations to features of the material microstructure.   The effects of the material microstructure on the progression of damage, and the state of local damage at the proportional limit stress (the stress level where the stress-strain curves deviates from linearity) were also a focus of that study. To simulate the progressive damage response, several continuum damage mechanics models provided in the ABAQUS finite element program which were appropriate for ceramic composites were tried. These models are based on Hashin's damage initiation criteria and the damage evolution is based on energy dissipation. However, serious convergence issues were encountered and no credible results could be obtained. While a damage mechanics type of model would be more representative of the actual material behavior, as a first approximation an elastic-perfectly plastic material model was used to analyze the initiation ('yielding') and damage progression ('inelastic flow') in the composite. A von Mises yield surface, which allows for isotropic yield, was used for all of the composite constituents. This criterion allows for limited redistribution of stresses as the stresses above the cracking stress (here idealized as a yield stress) are redistributed to the lower stress regions. It was seen that even this simple damage model provides results that are in good agreement with experimental data for the macro stress-strain response.   The maximum allowable strain in the x-direction (loading direction) for each constituent was initially set as follows: 0.06% for matrix, 0.05% for the transverse tows and 0.1% for the longitudinal tows based on the judgment of the authors and the available constituent data. These strain values translated to a maximum allowable stress of 36.6 ksi (252 MPa) for the matrix, 37.6 ksi (260 MPa) for the longitudinal tows, and 7.65 Ksi (53 MPa) for the transverse tows. The yield stress for each constituent was assumed to be the failure stress or the maximum allowable stress. As mentioned earlier, on attaining the yield stress, the constituents were assumed to be perfectly plastic (i.e., the stress in the constituent remained constant at its yield stress even as the strain increased, thereby inducing local stress redistribution). In addition, the maximum allowable stresses and strains for each constituent were chosen to reflect the fact that experimental results show that the longitudinal tows fail well after the matrix and transverse tows fail. Tensile stress-strain curves of a few of the actual sections were generated and are plotted along with an

experimentally obtained stress-strain curve[6] for comparison in Fig. 5. The section numbers shown in the figure are designated based on the sequence of sections taken from the specimen. As can be seen from this figure, each of the
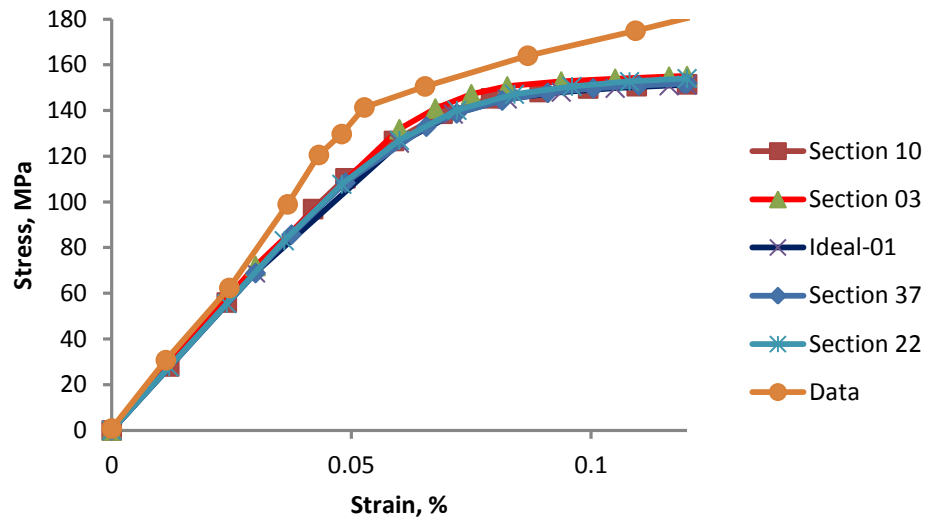

Figure 5. Experimental and computed stress-strain response of SiC/SiC composite

simulated stress-strain curves for the actual sections were nearly identical. The computed stress-strain curves showed an initial linear region, and a transition to a second linear region, with a shallower slope. The transition began at a strain level of around 0.036% and ended at a strain level of about 0.072%. This shows that the damage initiates well before the first major point of macroscopic non-linearity. This has also been substantiated experimentally by using acoustic emission technique to identify damage[7]. It was noticed that damage initiates well before the first point of observed non-linearity at the macro scale. It is also observed that very little local damage results in macroscopic non-linear stress-strain behavior. Even though, the overall stress-strain behavior in all sections was nearly identical, the local damage pattern and amount of damage in each section is different and the damage progression seems to follow the microstructural features of a given section. Damage seems to initiate where transverse tows are close together and it also seems to be concentrated around areas of large pores and near the damaged transverse tows. In addition, matrix damage appears to make vertical bands through the cross-section. Globally, the stress and strain levels at which the initial nonlinearity occurs in the stress-strain response were reasonably well predicted. The overall character of the computed stress-strain curves matches the experimental results, however. Note that the magnitude of local stress field at a point are highly mesh sensitive and therefore should not be viewed as a quantitatively precise value. In this work, no mesh dependence study was performed to assess the sensitivity of stress values. Sections were analyzed for damage initiation and progression and observing damage patterns.

As mentioned before, in order to model the damage behavior of constituents in a manner that is more representative of their actual behavior, matrix and transverse tows were modeled as brittle materials i.e. their stress-strain behavior was modeled as linear till failure. This is a very simple damage model. Once the stress in a constituent reaches the failure stress, the stiffness of that constituent is reduced to near zero. A simple user subroutine is written as a user-routine UMAT that is run with ABAQUS finite element code. This type of material behavior poses challenges in finding converged numerical solutions. A solution technique known as implicit-dynamic in the ABAQUS finite element code was used. Displacement was applied to the model using the *DYNAMIC keyword in ABAQUS with the parameter APPLICATION = QUASI-STATIC. This implicit dynamic solver is recommended for quasi-static problems exhibiting a high-degree of non-linearity. This procedure uses numerical damping to stabilize the problem. The numerical damping does not significantly affect the simulation results because the velocities in these simulations are low. This technique has advantages over traditional static, implicit solvers which have difficulty converging when the material exhibits post-peak softening.

However, it was noticed that in order to match the macroscopic stress-strain behavior to the observed data as well as the behavior using elastic-plastic analyses, the strength of the matrix and transverse tows had to be doubled. In brittle failure, large amount of stresses are redistributed following failure which may lead to rapid failure of the neighboring elements. Failure initiation generally leads to rapid failure progression. On the other hand, in the elastic-plastic analyses, since the material continues to carry the failure stress, the stress redistribution is very limited. The stress-strain behavior from the analysis of section 22 is shown in Fig. 6 as a very representative figure of the sections analyzed. As shown in the figure, using the previous (original) strength values for matrix and transverse tows would result in a much more compliant behavior. The matrix strength value, when doubled, of 505 MPa (73 Ksi) is more realistic and closer to the strength value for the bulk material.

Results from damage initiation and progression are presented here for only two sections mainly for the sake of brevity. Damage patterns are compared for these sections at three applied strain levels 0.036%, 0.054% and 0.072%. It is worth noting that the proportional limit stress (where macroscopic stress-strain curve deviates significantly from linear behavior) occurs at around a strain level of 0.06%. Figures 7-12 show the damage patterns in transverse tows and matrix regions of section 10 at applied strain levels of 0.036%, 0.054% and 0.072% respectively. It is seen from the figures that when constituents are assumed brittle with twice the strength values, the extent of damage at a given strain level is much less as compared to when the constituents were assumed elastic-plastic. This is due to the fact that in brittle materials, a large amount of stress (and thus the energy) needs to be redistributed upon failure, while in elastic-plastic materials, there is a very limited level of stress redistribution as the material constituents continue to carry the yield stress upon failure as also mentioned previously. Similar analyses were performed for section 22 and those results for damage distribution are shown in Figs. 13-18 for two types of material behaviors i.e. elastic-plastic and brittle. Again, for brittle constituents, the strength of the matrix and the transverse tows had to be doubled to match the macroscopic stress-strain behavior to the experimental data. Similar types of observations can be made from the results obtained for section 22. It was also observed that in the analyses
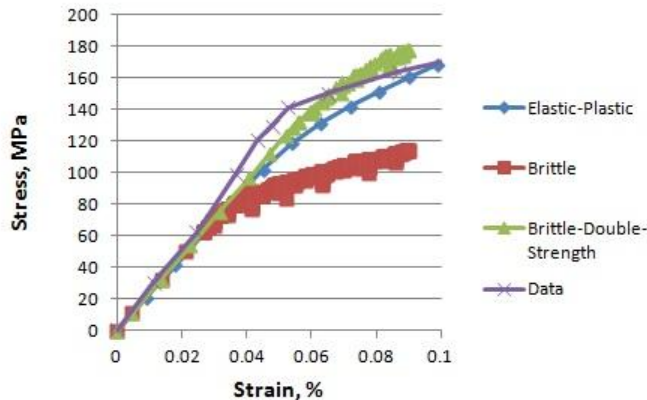

Figure 6. Stress-strain behavior of section 22

where material constituents were assumed brittle, the relationship of damage initiation and progression to the microstructural features remained same i.e. the damage tends to initiate where the transverse tows are bunched together and near the areas of large pores. Similar damage patterns, in relation to microstructural features, were also observed when constituents material behavior was assumed elastic-perfectly plastic.

IV. Conclusion

Detailed finite element analyses of a SiC/SiC woven material system architecture were performed. Methods were developed to generate detailed high quality images of those microstructures and then develop detailed finite element models from those images. Initially, constituent material behavior was assumed to be elastic-perfectly plastic and later on analyses were performed where the constituent materials were assumed brittle. Material strengths, where the constituents were assumed to be brittle, had to be doubled in order to match the macroscopic stress-strain response to the measured data. The damage pattern for both set of analyses for a given section was similar, but the amount of damage at a given strain level was different. Damage was always found to start in transverse tows and progress to vertical bands of matrix damage aligned with the damage in transverse tows. While the specific locations where these damage patterns occurred differed between various sections, the overall pattern in

the initiation and development of damage were similar. The damage initiation and progression appears to be related to the architectural and microstructural details of the sections analyzed. Future work will include incorporation of more realistic composite architectures, including non-uniform matrix thickness.

References

[1]Nemeth, N. N., Mital, S. K., and Lang, J., "Evaluation of Solid Modeling Software for Finite Element Analysis of Woven Ceramic Matrix Composites," NASA/TM-2010-216250, June 2010.

[2]Mital, S. K., Bednarcyk, B. A., Arnold, S. M., and Lang, J., "Modeling of Melt-Infiltrated SiC/SiC Composite Properties,", NASA/TM-2009-215806, October 2009.

[3]Goldberg, R. K., , Bonacuse, P. J., and Mital, S. K., "Investigation of Effects of Material Architecture on the Elastic Response of a Woven Ceramic Matrix Composite," NASA/TM-2012-217269, January 2012.

[4]Reid, A. C., Lua, R. C., Garcia, R. E., Coffman, V. R., and Langer, S. A., "Modelling Microstructures with OOF2," *International Journal of Materials and Product Technology*, Vol. 35, No. 3-4, 2009, pp. 361-373.

[5]ABAQUS Software Package, Ver. 6.8, SIMULIA, Providence, RI.

[6]Kiser, J., Calomino, A., Brewer, D., DiCarlo, J., and Morscher, G., "SiC/SiC Composites for High Temperature Applications," Proceedings of 7th International Conference on High Temperature Ceramic Matrix Composites, Sep. 19-22, 2010, Bayreuth, Bavaria, Germany.

[7]Morscher, G., "Stress, Matrix Cracking, Temperature, Environment and Life of SiC/SiC Woven Composites," Proceedings of 7th International Conference on High Temperature Ceramic Matrix Composites, Sep. 19-22, 2010, Bayreuth, Bavaria, Germany.

American Institute of Aeronautics and Astronautics
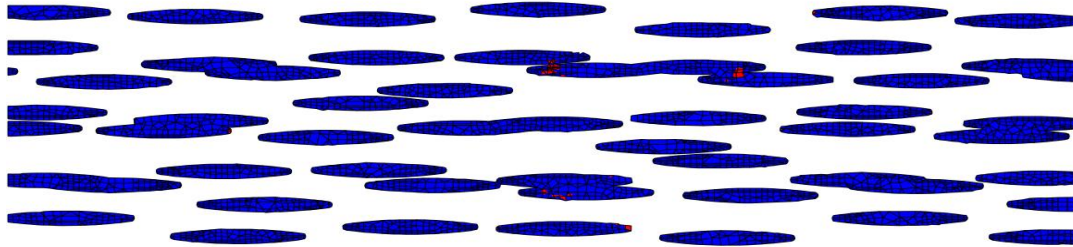
(a) Constituents assumed elastic-plastic
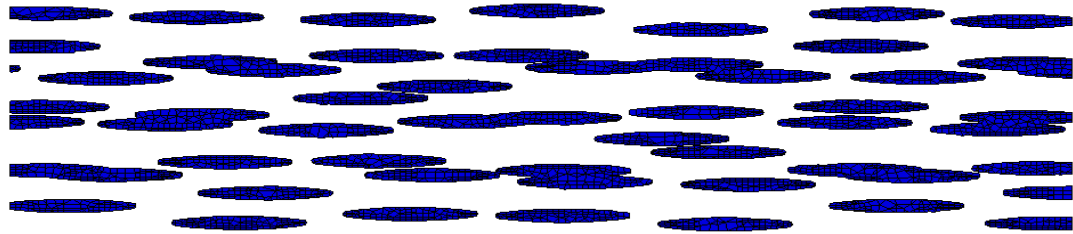
(b) Constituent assumed brittle

Figure 7. Areas in transverse tows in Section 10 at applied strain of 0.036% where stress levels exceed the failure stress indicated by red color and below the failure indicated by blue color.
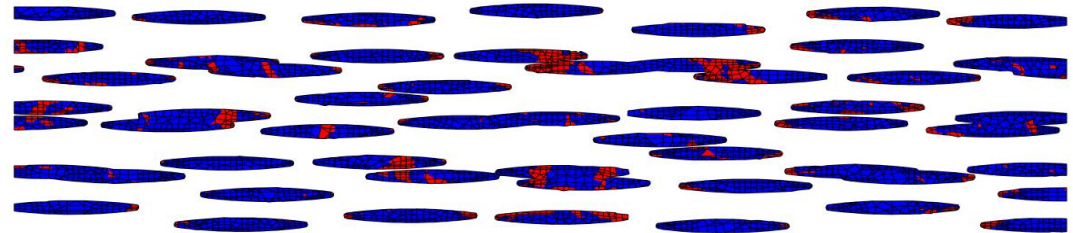

(a) Constituents assumed elastic-plastic
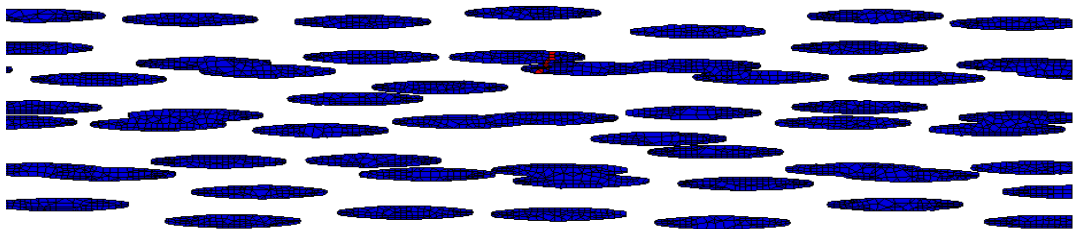
(b) Constituent assumed brittle

Figure 8. Areas in transverse tows in Section 10 at applied strain of 0.054% where stress levels exceed the failure stress indicated by red color and below the failure stress indicated by blue color.
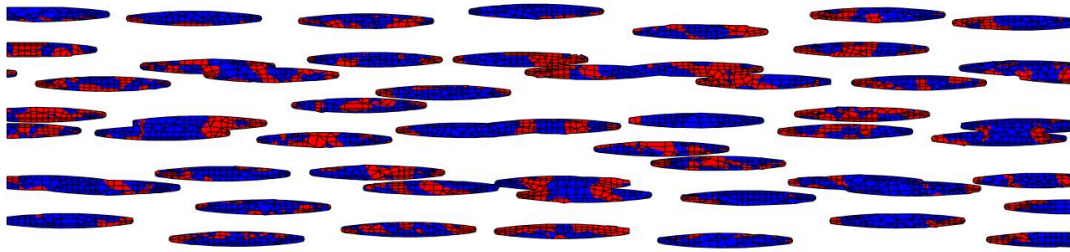
(a) Constituent assumed elastic-plastic
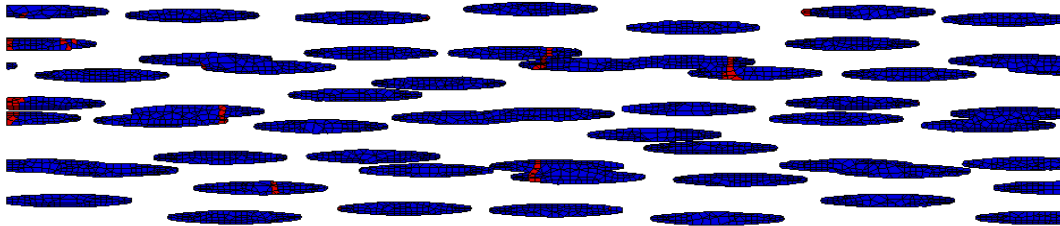
(b) Constituent assumed brittle

Figure 9. Areas in transverse tows in Section 10 at applied strain of 0.072% where stress levels exceed the failure stress indicated by red color and below the failure stress indicated by blue color.
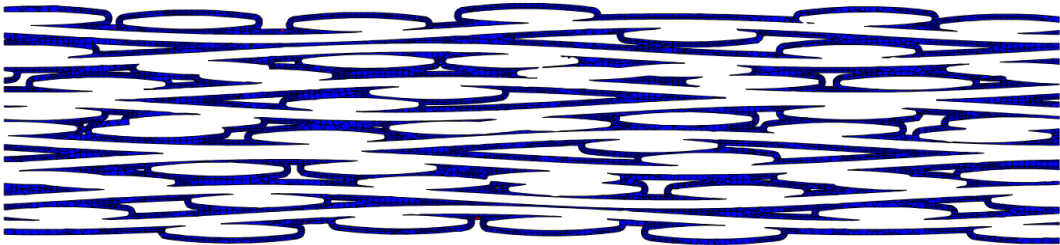
(a) Constituents assumed elastic-plastic
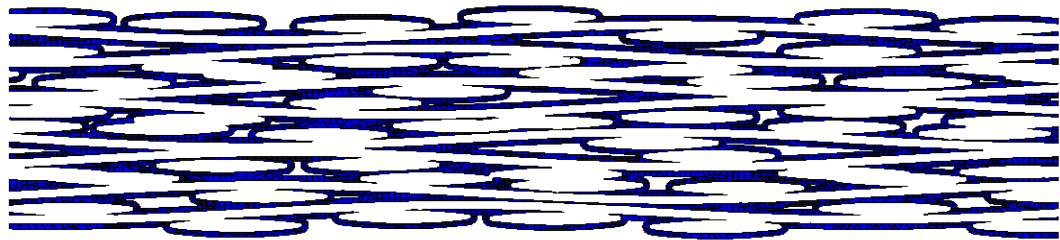
(b) Constituents assumed brittle

Figure 10. Areas of matrix region in Section 10 at applied strain of 0.036% where stress levels exceed the failure stress indicated by red color and below the failure stress indicated by blue color.
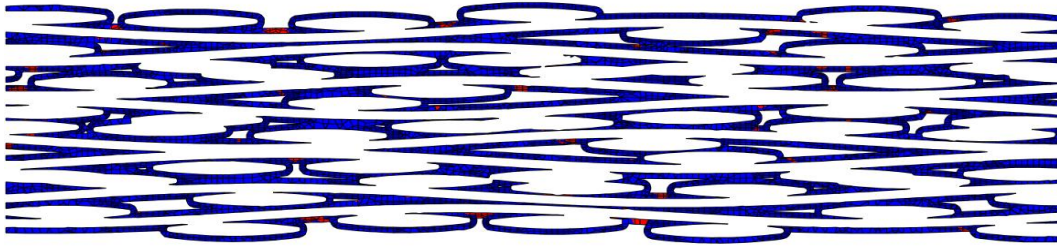
(a) Constituents assumed elastic-plastic
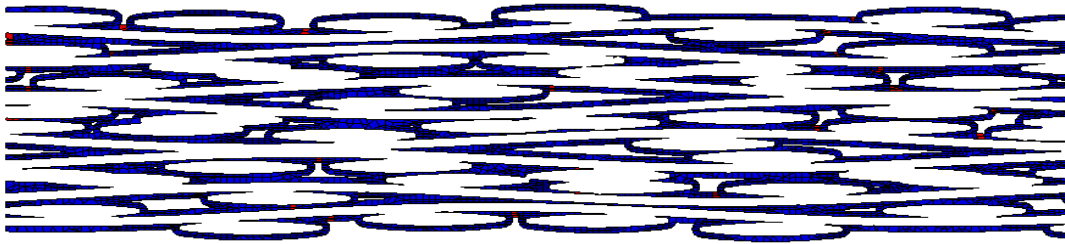
(b) Constituents assumed brittle

Figure 11. Areas of matrix region in Section 10 at applied strain of 0.054% where stress levels exceed the failure stress indicated by red color and below the failure stress indicated by blue color.
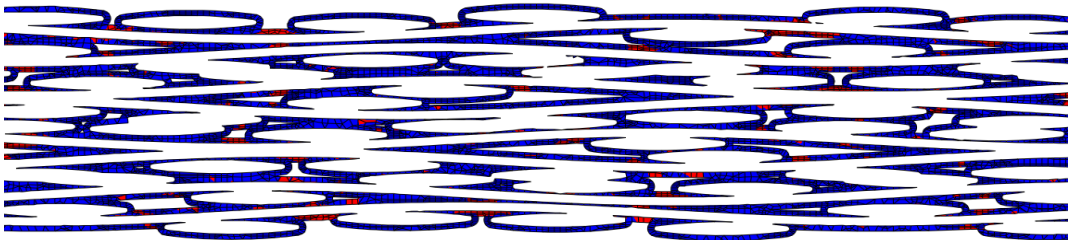
(a) Constituents assumed elastic-plastic
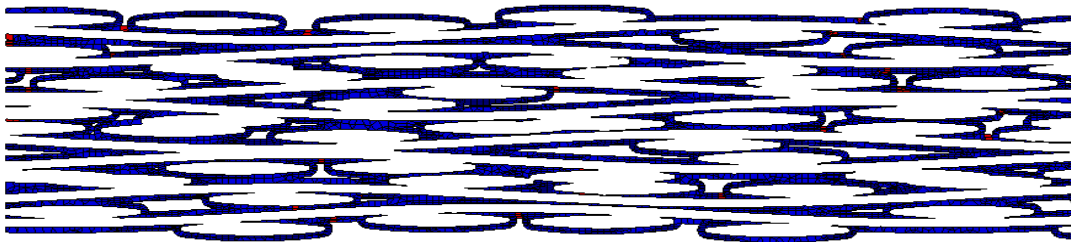
(b) Constituents assumed brittle

Figure 12. Areas of matrix region in Section 10 at applied strain of 0.072% where stress levels exceed the failure stress indicated by red color and below the failure stress indicated by blue color.
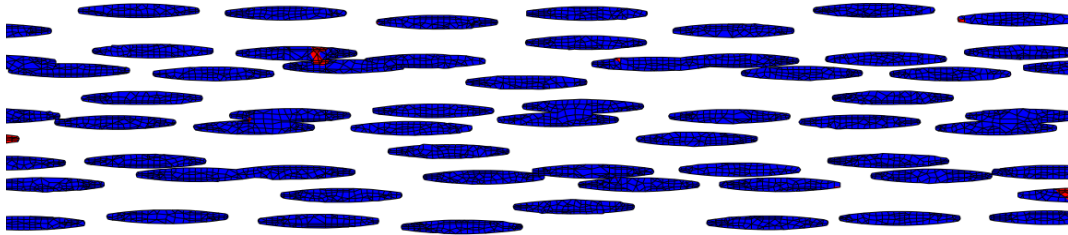
(a) Constituents assumed elastic-plastic
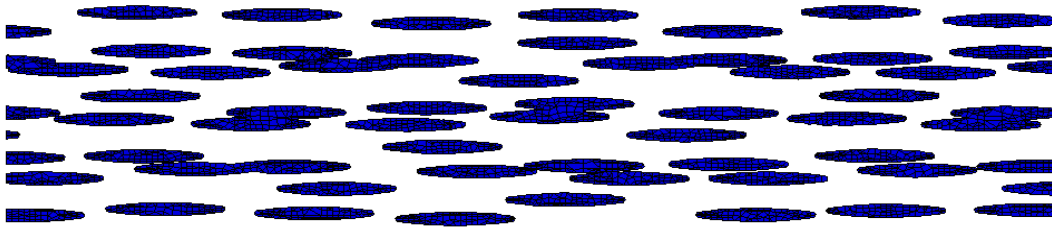
(b) Constituent assumed brittle

Figure 13. Areas in transverse tows in Section 22 at applied strain of 0.036% where stress levels exceed the failure stress indicated by red color and below the failure indicated by blue color.
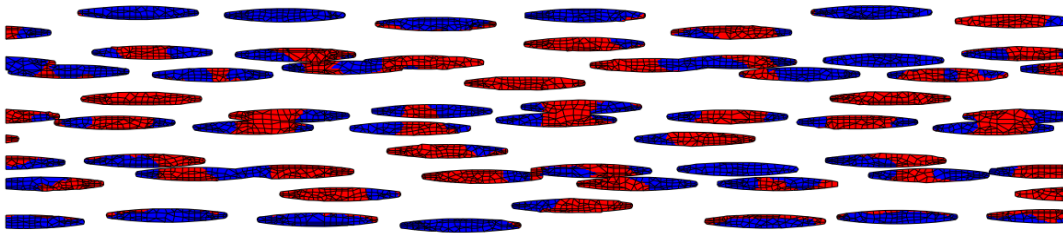

(a) Constituents assumed elastic-plastic
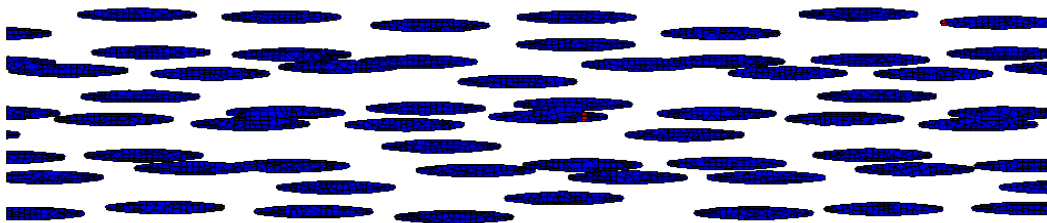
(b) Constituent assumed brittle

Figure 14. Areas in transverse tows in Section 22 at applied strain of 0.054% where stress levels exceed the failure stress indicated by red color and below the failure stress indicated by blue color.
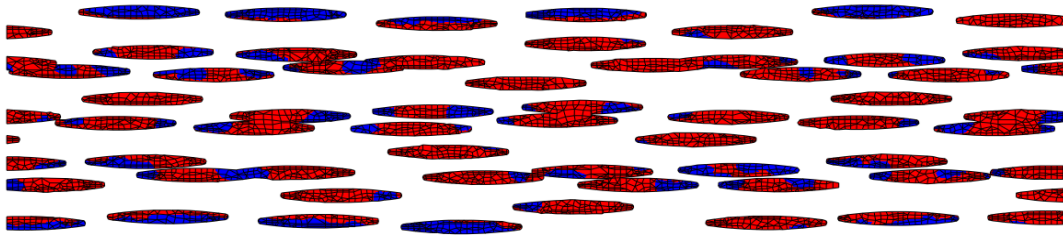
(a) Constituent assumed elastic-plastic
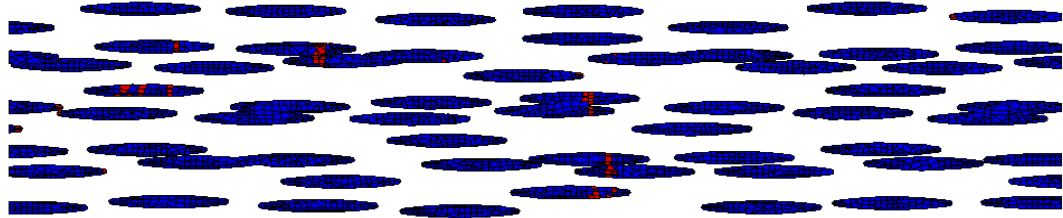
(b) Constituent assumed brittle

Figure 15. Areas in transverse tows in Section 22 at applied strain of 0.072% where stress levels exceed the failure stress indicated by red color and below the failure stress indicated by blue color.
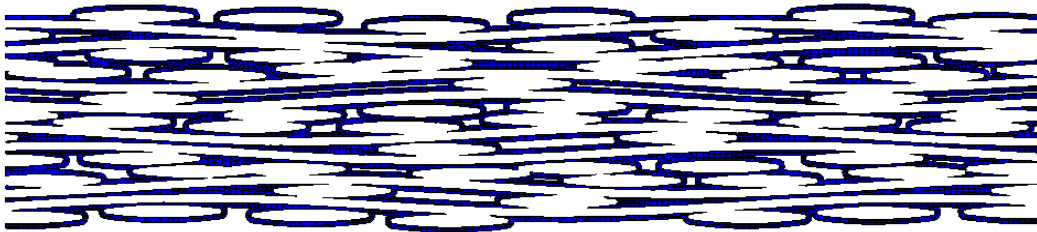

(a) Constituents assumed elastic-plastic

(b) Constituents assumed brittle

Figure 16. Areas of matrix region in Section 22 at applied strain of 0.036% where stress levels exceed the failure stress indicated by red color and below the failure stress
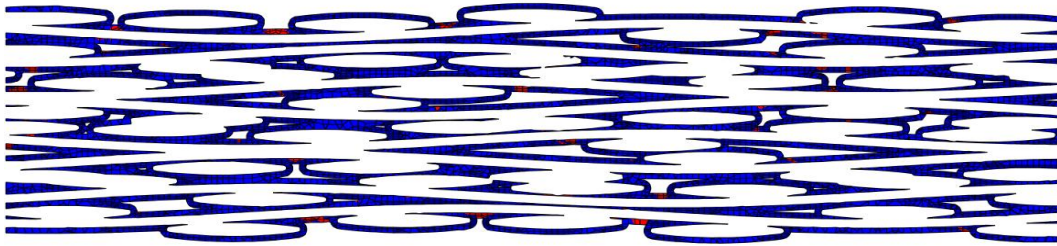
(a) Constituents assumed elastic-plastic
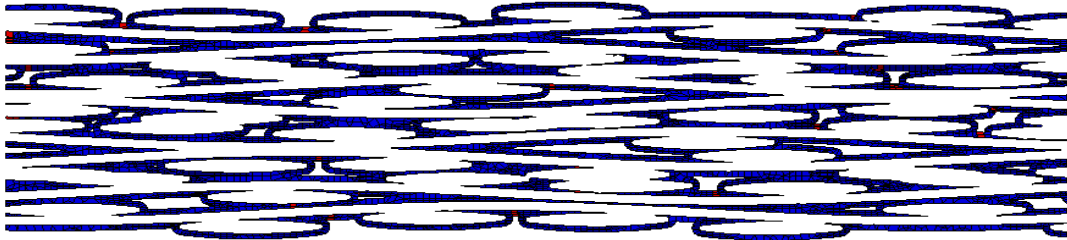
(b) Constituents assumed brittle

Figure 17. Areas of matrix region in Section 10 at applied strain of 0.054% where stress levels exceed the failure stress indicated by red color and below the failure stress indicated by blue color.
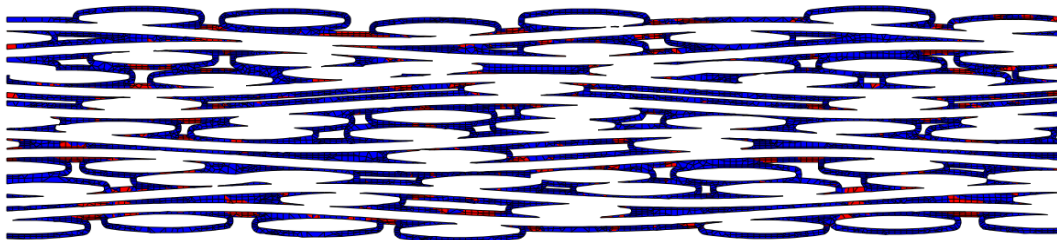
(a) Constituents assumed elastic-plastic
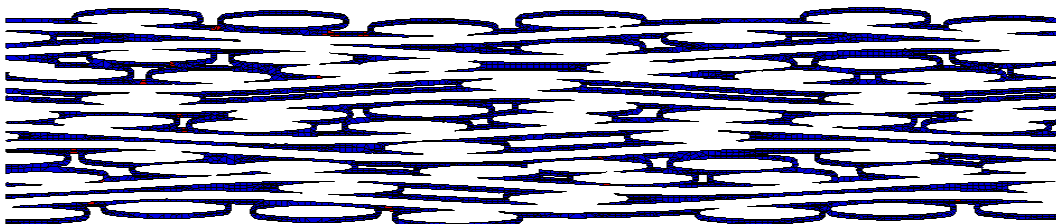
(b) Constituents assumed brittle

Figure 18. Areas of matrix region in Section 22 at applied strain of 0.072% where stress levels exceed the failure stress indicated by red color and below the failure stress indicated by blue color.